ECS Journal of Solid State
Science and Technology

Optoelectronic Properties of a Benzodithiophene-Based Organic Photovoltaic

ECS Journal of Solid State Science and Technology, 2021 **10** 075003

Optoelectronic Properties of a Benzodithiophene-Based Organic Photovoltaic

Yu-Wei Su,[1,z] Yi-Shan Huang,[1] Ho-Chun Huang,[1] and Po-Tuan Chen[2]

[1]*Department of Chemical Engineering, Feng Chia University, Taichung 40724, Taiwan*
[2]*Department of Vehicle Engineering, National Taipei University of Technology, Taipei 10608, Taiwan*

Benzo[1,2-b:4,5-b′]dithiophene (BDT) contains electron donating groups and conjugates with acceptor material as a donor-acceptor type conjugated polymer, which can be applied in bulk heterojunction organic photovoltaics due to its high charge carrier mobility. In this study, we used Stille coupling polymerization to synthesize a BDT monomer with thiophene side-chains and copolymerized with dioctyl 2,5-dibromoterephthalate (DTP) to form a 2-D type donor-acceptor conjugated polymer, BDT-DTP. Thermal analyses indicated that BDT-DTP has a high thermal decomposition temperature of 342.07 °C (weight loss = 5%), showing excellent thermal stability. The active layer comprised of BDT-DTP:3,9-bis(2-methylene-(3-(1,1-dicyanomethylene)-indanone))−5,5,11,11-tetrakis(4-hexylphenyl)-dithieno[2,3-d:2′,3′-d′]-s-indaceno[1,2-b:5,6-b′]dithiophene (ITIC) blended film in a OPV device could achieve a power conversion efficiency of 1.08%, open-circuit voltage of 0.88 V, short-circuit current density of 4.08 mA cm^{-2}, and fill factor of 30.1%. This work demonstrates a novel structure of benzodithiophene-based donor material used in the photovoltaic application.

 [DOI: 10.1149/2162-8777/ac12b4]

Manuscript submitted April 27, 2021; revised manuscript received June 29, 2021. Published July 15, 2021. *This paper is part of the JSS Focus Issue on Solid State Electronic Devices and Materials.*

Supplementary material for this article is available online

Organic photovoltaics (OPV) with a single-layer bulk heterojunction (BHJ) structure are cost-effective, lightweight, and simple to design for engineering, which has attracted widespread attention from both academia and industry.[1] In recent years, advancements in the application of donor polymers containing electron-donating moieties blended with non-fullerene acceptor materials have significantly improved the power conversion efficiency (PCE) of OPV to over 16%.[2–5] Abundant studies have focused on designing the donor materials based on electron donor-electron acceptor (D-A) alternating structures to regulate the highest occupied molecular orbital (HOMO) and the lowest unoccupied molecular orbital (LUMO) energy levels.[6–9] One-dimensional (1-D) conjugated polymers with repeating D-A units along the backbone of the main chain enables π-electron transfer along the backbone of the main chain, which will increase delocalized internal electron transfer. Subsequent derivatives include a branched D-A conjugated polymer formed by introducing strong electron-withdrawing groups to the side chains of the A unit and linking them to the D unit constituting the main chain. In the early time, two-dimensional (2-D) conjugated polythiophenes with bi(thienylenevinylene) side chains were designed and synthesized for application in OPV.[10] This conjugated polymer can absorb light from a wider range of visible light, which enhanced the hole mobility of the material to match the performance of previous polythiophene materials. Among them, molecules with good planarity and liability have been introduced in donor-type material designs, such as benzo[1,2-b:4,5-b′]dithiophene (BDT), cyclopentadithiophene, fluorene, indacenodithiophene, benzothiadiazole, and diketopyrrolopyrrole, which are structural polymeric units used to reduce the energy level and optical band gap of conjugated polymers in high-performance all-polymer solar cells.[11,12] The D-A type conjugated structure can promote the transfer of electrons from the side chains to the fullerene molecules to improve the electron affinity between molecules.[13,14] The π-conjugated side chains of the 2-D conjugated polymer can widen the conjugated plane, lower the HOMO energy level, and increase the open circuit voltage (V_{oc}) of the entire OPV device.[15] The optical band gap (E_g) determines the light absorption limit of a specific polymer and is a key parameter for the active layer material.[16]

In addition, the device's PCE is determined not only by the E_g of donor material but also by the polymer backbone configuration, which is directly associated with charge transport.[17–19] Previous studies have found that conjugated polymers with flexible side chains are more easily processed, but these side chains also hinder the closed packing of polymer backbones.[20–22] By modifying the conjugated side chains, the free-rotating single bonds in the polymer backbone can be further strengthened such as backbone torsion and amorphous aggregation.[23–25] In this study, the 2-D D-A conjugated polymer was synthesized using the Stille coupling method,[26–29] by which thiophene monomer side chains were added to BDT as the donor unit, followed by polymerization with dioctyl 2,5-dibromoterephthalate (DTP) monomer as the acceptor unit to form BDT-DTP polymer. There are two reasons for selecting DTP monomer as the acceptor. One is the low cost price of the staring material, 1,4-dibromo-2,5-dimethylbenzene (see Fig. S1 available online at stacks.iop.org/JSS/10/075003/mmedia), and the other one is the DTP-derivative as the key candidate for synthesizing a small molecule ITIC-FOR.[30]

Experimental

BDT-DTP polymerization.—Figure 1 shows the polymerization process of 2-D conjugated polymer BDT-DTP. Monomers M1 (97 mg, 0.09 mmol) and M2 (71 mg, 0.10 mmol) were used as the reactants and placed into a double-necked flask at a ratio of 1:1 with a reflux tube set up as above (see Fig. S1). Anhydrous toluene (3.0 ml) was used as the solvent, and tri-o-tolylphosphine ($P(o\text{-}tol)_3$) (3.15 mg, 8.0 mol%) and the catalyst tris(dibenzylideneacetone) dipalladium ($Pd_2(dba)_3$) (2.75 mg, 2 mol%) were added for Stille coupling. After the reaction was complete, methanol was slowly added while a stirrer bar was spinning at a fixed speed to obtain a brown precipitate (crude product). The orange-red solid product, polymer BDT-DTP, was obtained after washing out the low-molecular-weight oligomers and small molecules.

Materials characterizations.—A 2.0 mg of BDT-DTP was dissolved in 1 ml of tetrahydrofuran (THF) as an eluent injected into the gel permeation chromatography (GPC) system (Smartline, Jasco RI 930) with an Ultrahydrogel column (linear, 10 μm, 7.8 mm × 300 mm, 500 − 10 M). The polymer retention time were recorded, and the signals were analyzed to determine the average molecular weight and molecular weight distribution. A thermogravimetric

[z]E-mail: yuwsu@mail.fcu.edu.tw

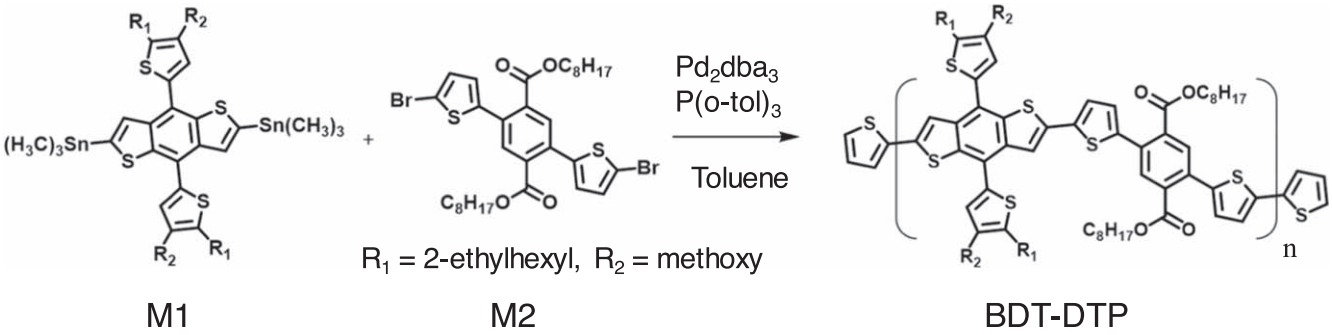

Figure 1. The polymerization process of 2-D conjugated polymer BDT-DTP.

analyzer (TGA; TA Instrument, TGA2950) was used to observe the thermal decomposition temperature (T_d) of BDT-DTP polymer under nitrogen at a heating rate of 10 °C min^{-1}. Cyclic voltammetry (CV; CH Instruments 6116E) was used to measure the oxidation and reduction potential of the BDT-DTP polymer to determine the HOMO and LUMO energy level values. The UV–vis adsorption spectrums of BDT-DTP:ITIC and BDT-DTP:$PC_{71}BM$ blended solutions and films were recorded between the wavelengths of 300−750 nm by a spectrometer (Ocean Optics HR4000). The blended ratio of polymer:small molecules was fixed at 1:1 (10 mg ml^{-1}: 10 mg ml^{-1}) and 1:1.5 (10 mg ml^{-1}: 15 mg ml^{-1}).

Device fabrication and measurement.—OPV devices were fabricated with the inverted structure of glass/indium tin oxide (ITO)/ZnO/BDT-DTP:ITIC/MoO_3/silver (Ag). The ZnO precursor was prepared by dissolving 100 mg of zinc acetate dihydrate (Aldrich, 99.9%) and 27 μl ethanolamine (Aldrich, 99.5%) in 1 ml 2-methoxyethanol (Aldrich, 99.8%) under vigorous stirring at 60 °C for 12 h to the hydrolysis reaction in air. Then, the ZnO precursor was spin casted at a rotating speed of 4000 rpm for 40 s on these ITO glass substrates and annealed at 150 °C for 20 min. The blend solution of the active layer was prepared by dissolving BDT-DTP (10 mg ml^{-1}) with ITIC (15 mg ml^{-1}) in chlorobenzene (CB) and stirred continuously for 12 h at 80 °C to completely dissolve the BDT-DTP and ITIC. The BHJ active layer was made by spin casting the blend solution. In order to optimize the device performance, the thickness of the BHJ active layer was tuned by setting different rotating speeds of 800, 1000, 1200, and 1400 rpm. After drying in ambient condition, a hole transport layer of 10-nm thick MoO_3 and an anode electrode of 100-nm thick Ag were subsequently thermally deposited on top of the BDT-DTP:ITIC blended films to complete the device fabrication. The device working area defined by the overlapping of ITO and Ag electrodes was 0.1 cm^2. The J–V characteristics were measured by using a Keithley 2400 source meter. The photocurrent was measured under simulated AM 1.5 G illumination at 100 mW cm^{-2} using a Xe lamp–based Newport 150 W solar simulator. The incident-photon-conversion efficiency (IPCE) spectra were collected using a setup composed of a lamp system, a chopper, a monochromator, a lock-in amplifier, and a standard silicon photodetector (ENLI Technology).

Grazing incidence wide angle X-ray scattering (GIWAXS) analysis.—GIWAXS analyses was performed for BDT-DTP:ITIC and BDT-DTP:$PC_{71}BM$ blended films in the BL23A station of the National Synchrotron Radiation Research Center (NSRRC) Hsinchu, Taiwan. The reason to probe the BDT-DTP:$PC_{71}BM$ blended film is to investigate the morphology condition influenced by the fullerene-type electron-withdrawing material. The experiment was conducted under an X-ray beam energy of 10 keV ($\lambda = 1.24$ Å), incident angle of 0.5°, and with a sample-to-detector distance of 11.42 cm.

Results and Discussion

Figure 2 shows a typical GPC chromatogram of the BDT-DTP polymer, revealing that the number-average molecular weight (Mn) of the BDT-DTP polymer is 26,378 Da, the weight-average molecular weight (Mw) is 44,431 Da, and the polydispersity index (PDI) is 1.68. Figure 3 shows a TGA curve of BDT-DTP polymer in a nitrogen environment, and the T_d was approximately at 342.07 °C; prior to T_d, only 5 wt% loss was observed, indicating excellent

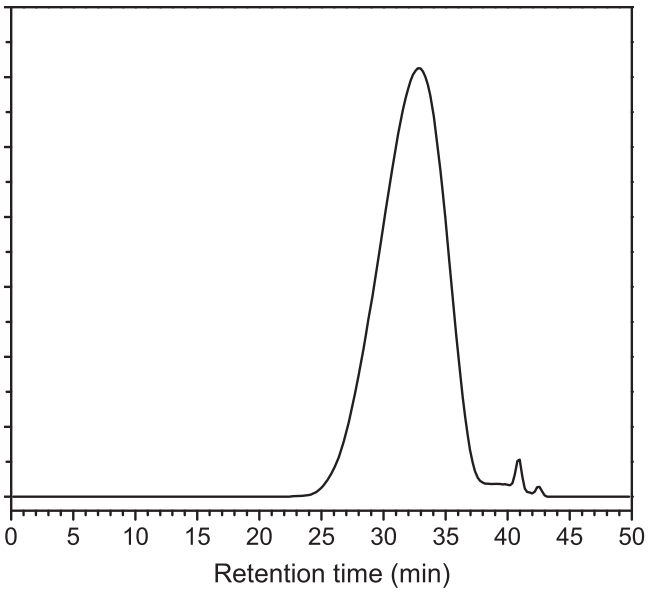

Figure 2. GPC chromatogram for molecular weight analysis of BDT-DTP polymer.

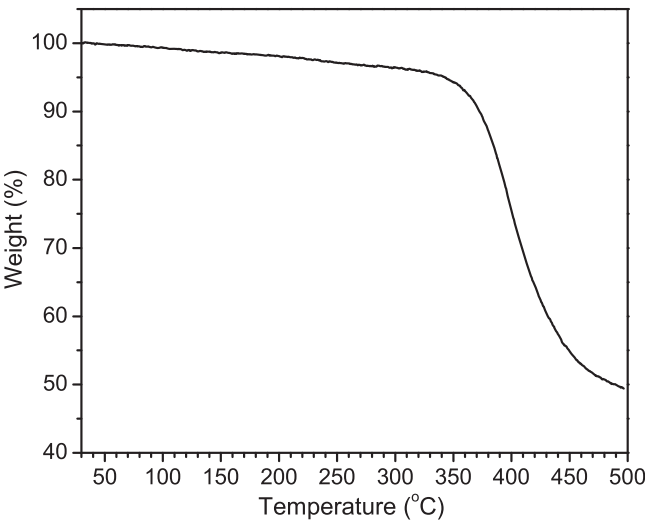

Figure 3. TGA curve of BDT-DTP polymer.

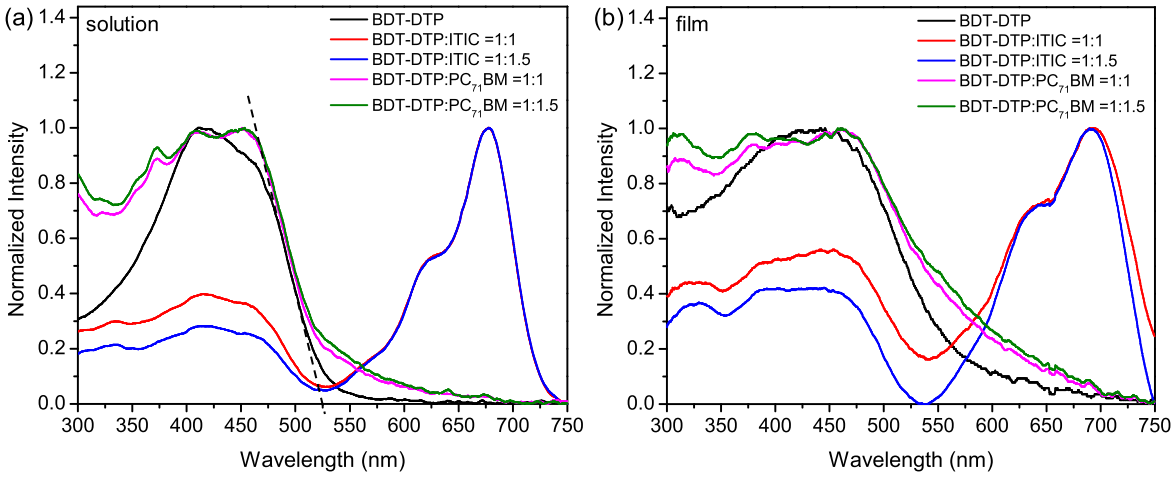

Figure 4. UV–vis absorption spectra of the BDT-DTP polymer, BDT-DTP:$PC_{71}BM$, and BDT-DTP:ITIC blends (a) in solution and (b) as a film.

thermal stability. The structure of the polymer began to decompose rapidly at a temperature above 400 °C.

Figures 4a and 4b present normalized UV–vis absorption spectra of the BDT-DTP polymer, BDT-DTP:$PC_{71}BM$, and BDT-DTP:ITIC blends in solution and in film, respectively. The BDT-DTP polymer in solution absorbed UV–vis light in the wavelength range of 350–500 nm, with a maximum absorption peak at 410 nm. In the solid film state, the shortened molecular distance increases the interaction forces between polymer chains, showing a slight red shift of a maximum absorption peak at 452 nm. The optical E_g of BDT-DTP in solution was determined by extrapolating the straight line (black dash line in Fig. 4a) on the UV–vis absorption edge value (λ = 525 nm) from absorption spectra and using the equation E_g (eV) = 1240/λ (nm), resulting a value of 2.36 eV. A blend system of BDT-DTP:$PC_{71}BM$ either in solution or film state shows a higher absorption range between 300–400 nm, which is contributed from the $PC_{71}BM$ molecules. The blended ratios of BDT-DTP:$PC_{71}BM$ in 1:1 and 1:1.5 present similar curve intensities. For the BDT-DTP:ITIC blend system, ITIC has the maximized absorption peak was at 678 nm in solution and 689 nm in solid film state. The absorption peaks of the blended film were red-shifted relative to that of the blended solution, indicating the agglomerate arrangement of ITIC in solid state. Comparing the BDT-DTP:$PC_{71}BM$ and BDT-DTP:ITIC blend systems, applying ITIC as the acceptor material in solution and solid states exhibit high absorption in visible-light range of 550−700 nm. Therefore, we speculate BDT-DTP:ITIC system could generate more effective excitons in OPV device.

Figure 5 shows the CV diagram of BDT-DTP polymer with a semi-reversible oxidation process. The applied potential scanned from the anode (cathode) could exhibit the first oxidation onset potential of the sample corresponding to the HOMO (LUMO) energy level value. The magnitude of the current was determined by the diffusion rate of the sample to the electrode surface. Therefore, when the electrode surface reaction approached completion, the diffusion rate was much smaller than the rate of change in applied potential and cause the current decreasing at this time. The oxidation potential of BDT-DTP polymer was 1.18 V and the calculated HOMO energy level was −5.98 eV based on the Eq. 1. In addition, the BDT-DTP polymer undergoes a semi-reversible reduction process showing a reduction potential at −1.25 V (relative to Fc+/Fc), and the calculated LUMO energy level was −3.55 eV based on the Eq. 2. The oxidation onset potential of ferrocene (Fc) was used as the reference relative to a vacuum level of −4.8 eV.

$$\mathrm{HOMO} = -\mathrm{e}(E_{ox} + 4.8) \quad [1]$$

$$\mathrm{LUMO} = -\mathrm{e}(E_{red} + 4.8) \quad [2]$$

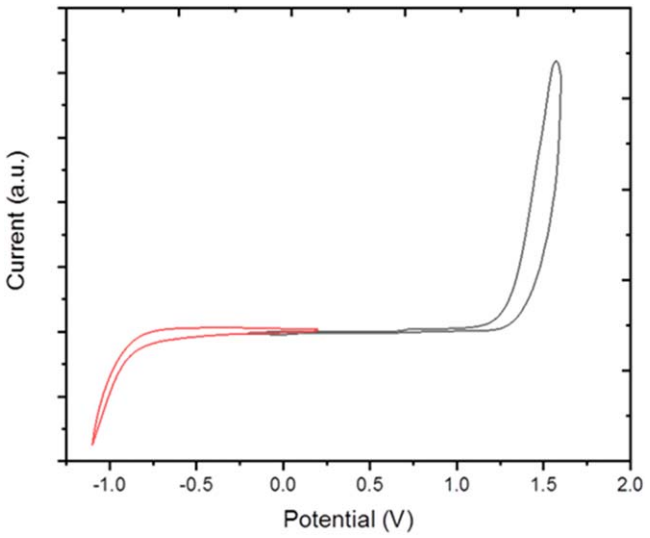

Figure 5. CV diagram of the BDT-DTP polymer.

Figure 6a presents a schematic representation of a BHJ OPV device with the electron transport layer (ZnO)/cathode (ITO) and hole transport layer (MoO_3)/anode (Ag) aligned vertically to the plane of the active layer. Upon the absorption of light, an exciton undergoes charge-transfer process at an ultrafast pace (ca. 100fs), and then the hole and electron remain in the donor and acceptor phases, respectively, held together through coulombic attraction. Figure 6b shows a schematic diagram of the HOMO-LUMO energy levels of the BDT-DTP polymer (obtained from CV), $PC_{71}BM$, and ITIC. The excitons induced by light are generated in BDT-DTP and then dissociated at the interfaces of BDT-DTP/ITIC and BDT-DTP/$PC_{71}BM$, due to a cascade alignment of HOMO and LUMO levels between these materials.

Figure 7a presents the J–V characteristics of OPV devices based on the inverted structure glass/ITO/ZnO/blend films/MoO_3/Ag. We only focus on the BDT-DTP:ITIC blend system, due to the inferior device performance achieved by BDT-DTP:$PC_{71}BM$ blend system with PCEs from $1.5 * 10^{-4}$ to $3 * 10^{-3}$%. (see Fig. S2 and Table SI). The device incorporating an active layer of BDT-DTP:ITIC spin-casted by 800 rpm, resulting in 108 nm thickness and showing an average PCE of 0.82%, J_{sc} of 3.08 mA cm^{-2}, V_{oc} of 0.89 V, and FF of 30.1%. Increasing the rotating speed to 1000 rpm can reduce the active layer in a thickness of 92 nm, and shows an average PCE of 0.98%, J_{sc} of 3.62 mA cm^{-2}, V_{oc} of 0.89 V, and FF of 30.4%. The optimized condition shows at a spin speed of 1200 rpm resulting in a

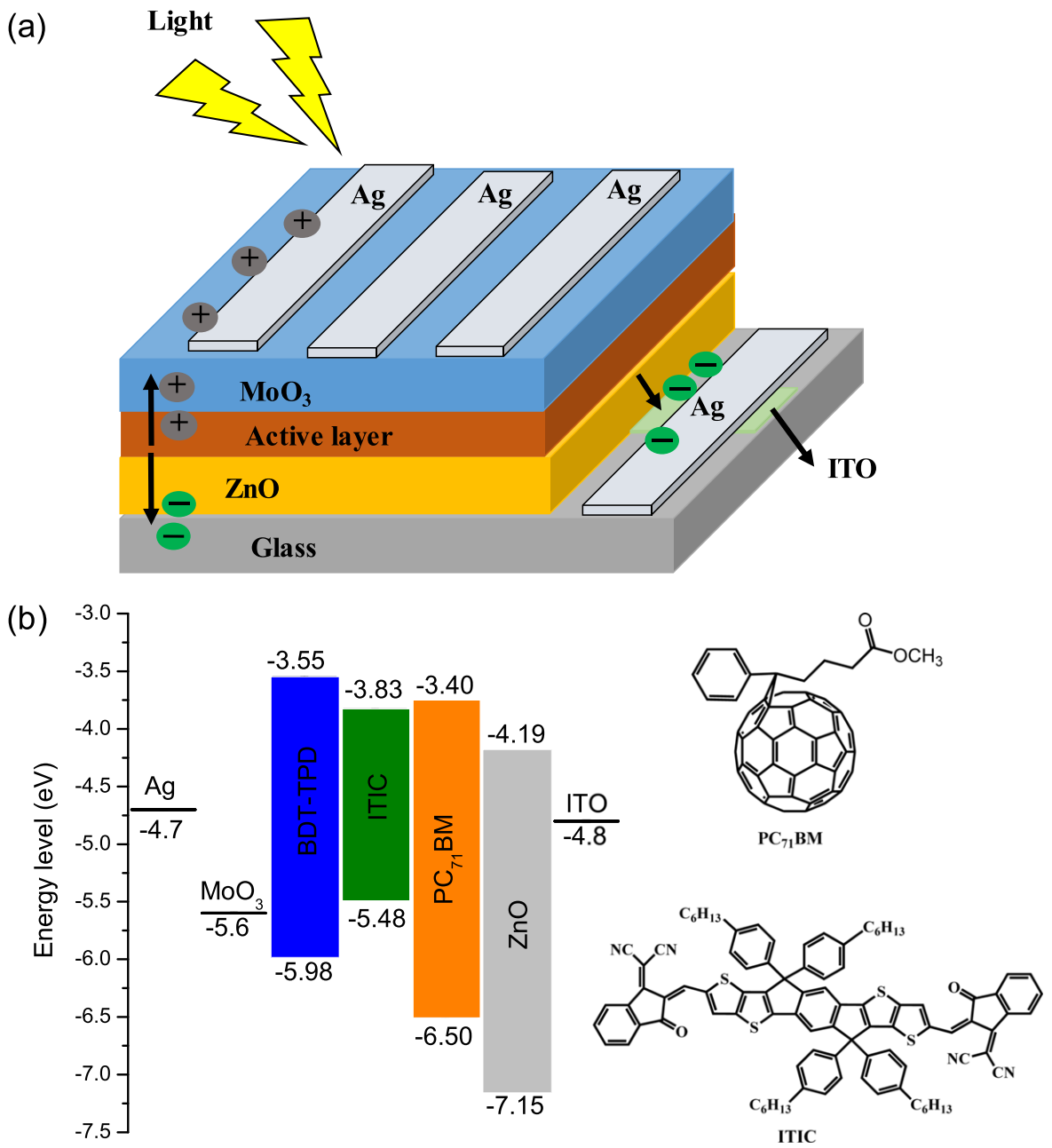

Figure 6. Schematic representations of (a) a BHJ OPV device structure and (b) HOMO-LUMO energy levels of the BDT-DTP polymer, $PC_{71}BM$, and ITIC.

86-nm thickness blended film can improve the average PCE to 1.08%, and obtain J_{sc} of 4.08 mA cm^{-2}, V_{oc} of 0.88 V, and FF of 30.1%. For the thinner active layer in a thickness of 76 nm, the device performance present decreased values of PCE in 0.95%, J_{sc} in 3.95 mA cm^{-2}, V_{oc} in 0.78 V, and FF of 30.9%. The improvement of J_{sc} is also confirmed by the IPCE spectra shown in Fig. 7b. Apparently, the 86-nm thickness blend film has the highest IPCE spectrum among these four devices with different film thickness. The highest IPCE values present at a range of 600–700 nm.

As the active layer thickness is increased, the decrease in the magnitude of the electric field would decrease the charge extraction performance, and this leads to a decrease in |Jsc| and FF, and an increase in the charge recombination.[31] On the other hand, a much thinner active layer could not absorb enough incident light for generating number of excitons for charge separation in donor/acceptor interfaces. We also applied atomic force microscopy (AFM) to scan the active layer surface. The root-mean-square (rms) surface roughness of BDT-DTP:ITIC active layer in a thickness of 108, 92, 86 and 76 nm are 2.51, 2.29, 1.93, and 1.66 nm, respectively (see Fig. S3). We suspect that the rms roughness increased as a result of the increased aggregation of the polymers.

Figures 8a–8c shows the 2-D GIWAXS scattering patterns of pristine BDT-DTP, BDT-DTP:$PC_{71}BM$ blend, and BDT-DTP:ITIC blend films, respectively. The color pixels represent scattering intensities from these organic thin films. Figure 9 shows the corresponding 1-D GIWAXS profiles in the out-of-plane (OP) direction (q_z, solid line) and in-plane (IP) direction (q_{xy}, dash line). In the pristine BDT-DTP film, microcrystals stacked in random orientations result in an (100) scattering peaks value of 0.31 $Å^{-1}$ in both OP and IP directions. In the BDT-DTP:$PC_{71}BM$ blend system, the (100) scattering peak of BDT-DTP presents a broaden shape and reduced intensity, indicating the alkyl-chain stacking destroyed by blending the $PC_{71}BM$ small molecules. A scattering peak at 1.34 $Å^{-1}$ indicates that a $PC_{71}BM$ exists in the stacking structure and disperses in the BDT-DTP polymer. For the BDT-DTP:ITIC film, the scattering peak values of 0.50 and 0.57 $Å^{-1}$ in OP direction

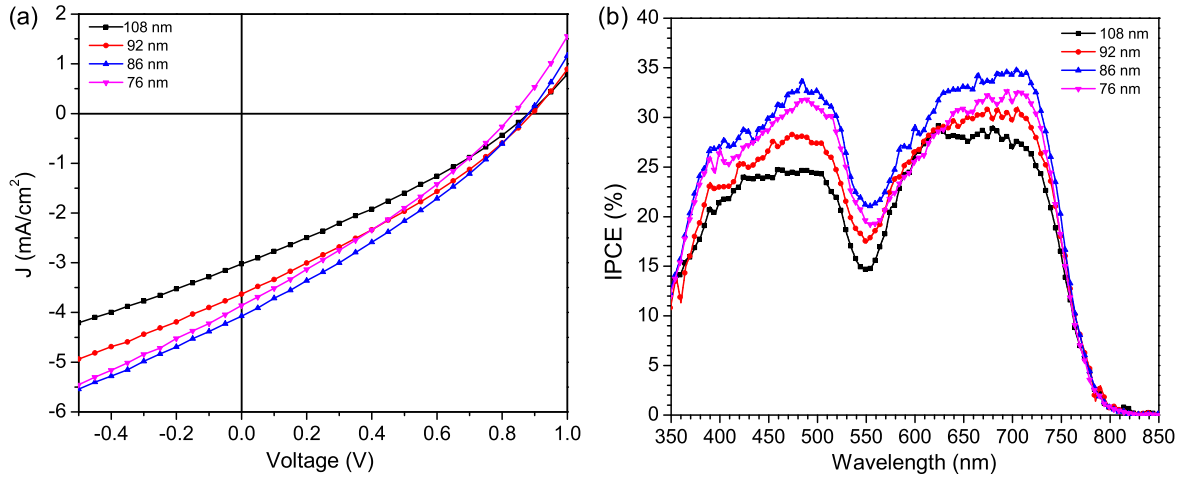

Figure 7. (a) J–V characteristics and (b) IPCE spectra of the devices comprising BDT-DTP:ITIC active layer in various thickness.

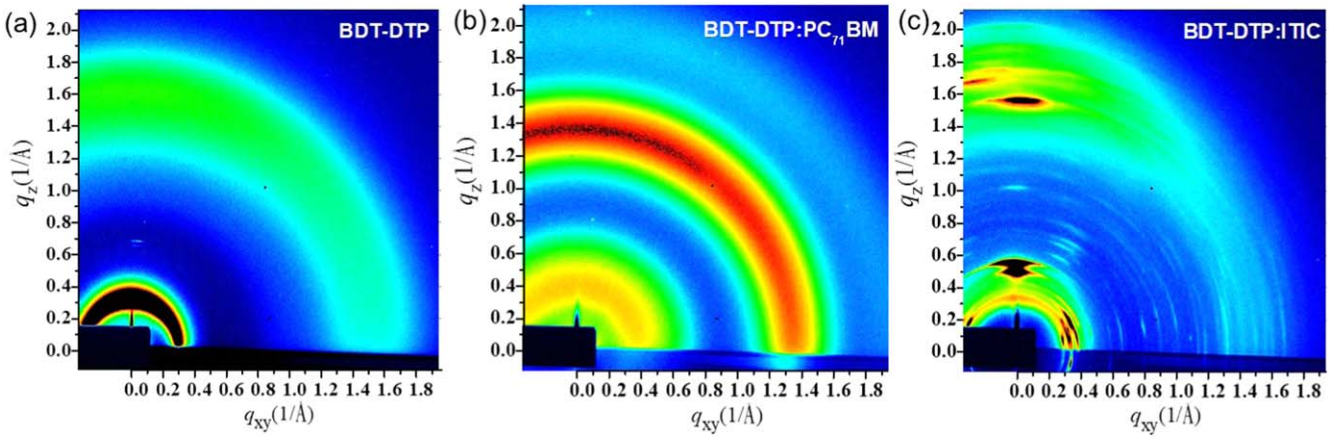

Figure 8. 2-D GIWAXS plots of pristine BDT-DTP film, BDT-DTP:PC71BM, and BDT-DTP:ITIC blended films.

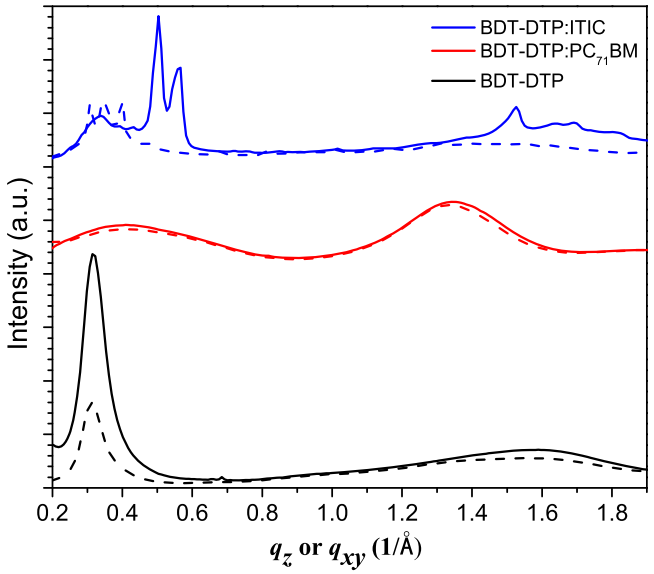

Figure 9. 1-D GIWAXS profiles of BDT-DTP polymer, BDT-DTP: PC71BM, and BDT-DTP:ITIC blended films in OP (solid line) and IP (dash line) directions.

represent the ITIC small molecule's stacking. The π-stacking signals of BDT-DTP polymer was found at 1.53 Å^{-1} lower than the 1.59 Å^{-1} in pristine BDT-DTP film, indicating the π-distance being enlarged from 3.95 to 4.10 Å (d = $2\pi/q$) due to the intercalating of small molecules in polymer lamella packing.

Conclusions

An alternating 2-D D-A conjugated polymer, BDT-DTP, was synthesized through the Stille coupling polymerization of BDT donor unit with thiophene-substituted side chains and DTP acceptor monomer unit. This 2-D D-A conjugated structure with substituted side chains in the direction perpendicular to the polymer backbone could also further enhance the delocalized π-electrons in the normal direction along the conjugated main chains. UV–vis spectra showed that the BDT-DTP polymer exhibited a maximum absorption peak at 410 nm, and a broadened absorption range from 300–400 nm when blended with $PC_{71}BM$. When blended with ITIC, the UV–vis absorption range could extend to 650–700 nm to absorb more light for generating excitons. The optimized condition of the OPV device comprised of BDT-DTP:ITIC blended film in 86-nm thickness exhibited a PCE of 1.08%, J_{sc} of 4.08 mA cm^{-2}, V_{oc} of 0.88 V, and FF of 30.1%. The 2-D GIWAXS scattering patterns showed the pristine BDT-DTP polymer has microcrystalline arrangement in the film, and the π-distance was enlarged from 3.95 to 4.10 Å due to the intercalating of ITIC small molecules in polymer lamella packing.

Acknowledgments

We acknowledge Mr Chung-Hao Chen, Dr Yu-Che Lin and Prof. Kung-Hwa Wei from Department of Materials Science and Engineering of National Yang Ming Chiao Tung University

provided organic synthesis technical supports. We also acknowledge the funding support from Ministry of Science and Technology (MOST) in Taiwan (MOST 106-2218-E-035-010-MY3 and 108-2113-M-027-008-MY2).

ORCID

Yu-Wei Su https://orcid.org/0000-0003-1303-7032
Ho-Chun Huang https://orcid.org/0000-0002-4424-3771

References

1. Y.-W. Su, S.-C. Lan, and K.-H. Wei, *Mater. Today*, **15**, 554 (2012).
2. B.-H. Jiang, Y.-P. Wang, C.-Y. Liao, Y.-M. Chang, Y.-W. Su, R.-J. Jeng, and C.-P. Chen, *ACS Appl. Mater. Interfaces*, **13**, 1076 (2021).
3. B. Chang, H.-W. Cheng, Y.-C. Lin, H.-C. Wang, C.-H. Chen, V.-T. Nguyen, Y. Yang, and K.-H. Wei, *ACS Appl. Mater. Interfaces*, **12**, 55023 (2020).
4. H.-W. Cheng et al., *Nano Lett.*, **21**, 2207 (2021).
5. L. Zhan, S. Li, T.-K. Lau, Y. Cui, X. Lu, M. Shi, C.-Z. Li, H. Li, J. Hou, and H. Chen, *Energy Environ. Sci.*, **13**, 635 (2020).
6. C. Cui and Y. Li, *Energy Environ. Sci.*, **12**, 3225 (2019).
7. J. Zhang, L. Zhu, and Z. Wei, *Small Methods*, **1**, 1700258 (2017).
8. G. Cai, Y. Li, J. Zhou, P. Xue, K. Liu, J. Wang, Z. Xie, G. Li, X. Zhan, and X. Lu, *ACS Appl. Mater. Interfaces*, **12**, 50660 (2020).
9. H.-W. Cheng et al., *ACS Appl. Mater. Interfaces*, **13**, 27227 (2021).
10. J. Hou, Z. Tan, Y. Yan, Y. He, C. Yan, and Y. Li, *J. Am. Chem. Soc.*, **128**, 4911 (2006).
11. C. Lee, S. Lee, G. Kim, W. Lee, and B. J. Kim, *Chem. Rev.*, **119**, 8028 (2019).
12. F.-C. Hsu, J.-W. Luo, Y.-W. Su, C.-S. Yang, Y.-A. Lin, J.-Y. Lin, C.-Y. Chang, Y.-F. Chen, and C.-P. Li, *ACS Appl. Energy Mater.*, **3**, 4217 (2020).
13. Y.-W. Su, Y.-C. Lin, and K.-H. Wei, *J. Mater. Chem. A*, **5**, 24051 (2017).
14. Z. Zhang and Y. Li, *Sci. China Chem.*, **58**, 192 (2015).
15. K. Zhang, Y. Qin, F. Li, L. Yu, and M. Sun, *J. Phys. Chem. C*, **121**, 19634 (2017).
16. K. Zhao, Q. Wang, B. Xu, W. Zhao, X. Liu, B. Yan, M. Sun, and J. Hou, *J. Mater. Chem. A*, **4**, 9511 (2016).
17. S. Ko et al., *Energy Environ. Sci.*, **10**, 1443 (2017).
18. K. Colladet et al., *Macromolecules*, **40**, 65 (2007).
19. Y. Gao, M. Liu, Y. Zhang, Z. Liu, Y. Yan, and L. Zhao, *Polymers*, **9**, 39 (2017).
20. J. Dou, Y. Zhen, T. Lei, S. Zhan, Z. Wang, W. Zhang, J. Wang, and J. Pei, *Adv. Funct. Mater.*, **24**, 6270 (2014).
21. B. Kang, R. Kim, S. B. Lee, S. Kwon, Y. Kim, and K. Cho, *J. Am. Chem. Soc.*, **138**, 3679 (2016).
22. L. Ye, X. Jiao, H. Zhang, S. Li, H. Yao, H. Ade, and J. Hou, *Macromolecules*, **48**, 7156 (2015).
23. Z. Yu, Y. Lu, J. Wang, and J. Pei, *Chem. Eur. J.*, **26**, 16194 (2020).
24. J. Lee, A. J. Kalin, T. Yuan, M. Al-Hashimi, and L. Fang, *Chem. Sci.*, **8**, 2503 (2017).
25. Y.-W. Su, C.-M. Liu, J.-M. Jiang, C.-S. Tsao, H.-C. Cha, U.-S. Jeng, H.-L. Chen, and K.-H. Wei, *J. Phys. Chem. C*, **119**, 3408 (2015).
26. M. R. Raj, M. Kim, H. I. Kim, G. Lee, C. W. Park, and T. Park, *J. Mater. Chem. A*, **5**, 3330 (2017).
27. Z. Ma, E. Wang, M. E. Jarvid, P. Henriksson, O. Ingänas, F. Zhang, and M. R. Andersson, *J. Mater. Chem.*, **22**, 2306 (2012).
28. Y.-C. Lin, H.-W. Cheng, Y.-W. Su, B.-H. Lin, Y.-J. Lu, C.-H. Chen, H.-C. Chen, Y. Yang, and K.-H. Wei, *Nano Energy*, **43**, 138 (2018).
29. C.-H. Chen, Y.-J. Lu, Y.-W. Su, Y.-C. Lin, H.-K. Lin, H.-C. Chen, H.-C. Wang, J.-X. Li, K.-H. Wu, and K.-H. Wei, *Org. Electron.*, **71**, 185 (2019).
30. M. Luo, Z. Zhang, L. Feng, H. Peng, L. Jiang, S. Xu, H. Li, F. Cai, Y. Li, and Y. Zou, *New J. Chem.*, **42**, 19279 (2018).
31. M. L. I. Ibrahim and H. A. Hassan, *IEEE Trans. Electron Devices*, **66**, 3124 (2019).